Supporting Information

Facile fabrication of hierarchical porous rose-like $NiCo_2O_4/MnCo_2O_4$ with enhanced electrochemical performance for energy storage

Yanjun Zhai[a], Hongzhi Mao[a], Peng Liu[a], Xiaochuan Ren[c], Liqiang Xu*[a] and Yitai Qian[ab]

[a]Key Laboratory of Colloid and Interface Chemistry, Shandong University, Ministry of Education, School of Chemistry and Chemical Engineering, Jinan 250100, China.

[b]Hefei National Laboratory for Physical Science at Microscale, Department of Chemistry, University of Science and Technology of China, Hefei 230026, China.

[c]Research Institute of Surface Engineering, Taiyuan University of Technology, Taiyuan, 030024, China

*Corresponding Author. Email: xulq@sdu.edu.cn, Tel. & Fax: +86 531 88364543.

Figure captions:

Fig. S1 (a, b) SEM, (c) TEM, (d) EDX mapping images of the Ni-Co-based precursors and (e) TEM of the Ni-Co-Mn-based precursors.

Fig. S2 Thermogravimetric analysis (TGA) of the as-prepared Ni-Co-Mn-based precursors.

Fig. S3 XRD patterns of as-prepared pure $NiCo_2O_4$.

Tab. S1 Some diffraction peaks of the prepared $NiCo_2O_4/MnCo_2O_4$, $NiCo_2O_4$, $NiCo_2O_4$ (JCPDS card no. 73−1702) and $MnCo_2O_4$ (JCPDS card no. 23−1237).

Fig. S4 Raman spectra of $NiCo_2O_4/MnCo_2O_4$ and $NiCo_2O_4$ excited with 473 nm laser.

Tab. S2 The Raman peak positions of the synthesized products and previously reported $NiCo_2O_4$, $MnCo_2O_4$ and manganese-based oxides.

Fig. S5 EDS spectrum of $NiCo_2O_4/MnCo_2O_4$.

Tab. S3 The interplanar spacing of the prepared $NiCo_2O_4/MnCo_2O_4$, $NiCo_2O_4$ (JCPDS card no. 73-1702) and $MnCo_2O_4$ (JCPDS card no. 23−1237).

Fig. S6 (a, b, c) TEM images, (d) HRTEM image and (e, f) SEM images of the as-prepared mesoporous $NiCo_2O_4$ hierarchical architectures.

Fig. S7 TEM images of the Ni-Co-based precursors synthesized at 180 ºC for (a, b) 40 min (c, d) 50 min, (e, f) 2.0 h, (g, h) 5.0 h, (i, j) 12.0 h and (k, l)15.0 h.

Fig. S8 TEM images of the Ni-Co-based precursors synthesized with different amounts of TEA: (a) 0 ml, (b) 3 ml, (c) 6 ml, (d) 10 ml at 180 ºC while keeping other experimental parameters unchanged; (e) the possible formation mechanism of the 3D hierarchical porous rose-like architectures.

Fig. S9 Nitrogen adsorption-desorption isotherm and the corresponding pore size distribution (inset) of (a) hierarchical porous rose-like $NiCo_2O_4$ and (b) hierarchical porous rose-like $NiCo_2O_4/MnCo_2O_4$.

Fig. S10 The first five cyclic voltammogram curves of the 3D hierarchical porous rose-like $NiCo_2O_4$.

Fig. S11 (a) CV curves of $NiCo_2O_4/MnCo_2O_4$ at different scan rate after 350 cycles and (b) logi vs. logv plots at different peaks.

Fig. S12 Cycling performance of $NiCo_2O_4/MnCo_2O_4$ with active materials of 70 % at 500 and 1000 mA g^{-1}.

Fig. S13 (a) Nyquist plots of the AC impedance spectra measured over the frequency ranging from 100 kHz to 0.01 Hz and (b, c) the direct current resistance (R_{dc}) for the $NiCo_2O_4/MnCo_2O_4$ and $NiCo_2O_4$ electrodes. (d) The AC impedance spectra of the $NiCo_2O_4/MnCo_2O_4$ after certain cycles at 1000 mA g^{-1} in the frequency ranging from 100 kHz to 0.01 Hz.

Fig. S14 (a) TEM image of the acetylene-black used as active material and (b) TEM image of $NiCo_2O_4/MnCo_2O_4$ composite used as active material (marked by the red frame) and acetylene-black acted as conductive agent after ten cycles at a current density of 1000 mA g^{-1}.

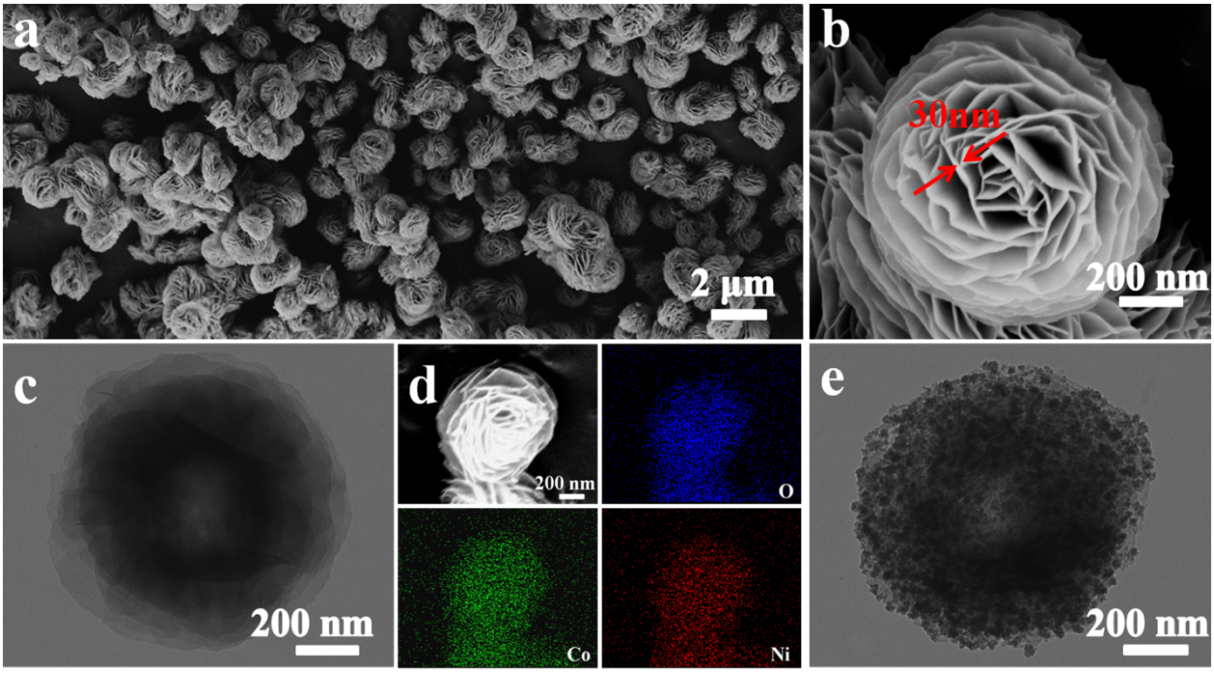

Fig. S1 (a, b) SEM, (c) TEM, (d) EDX mapping images of the Ni-Co-based precursors and (e) TEM of the Ni-Co-Mn-based precursors.

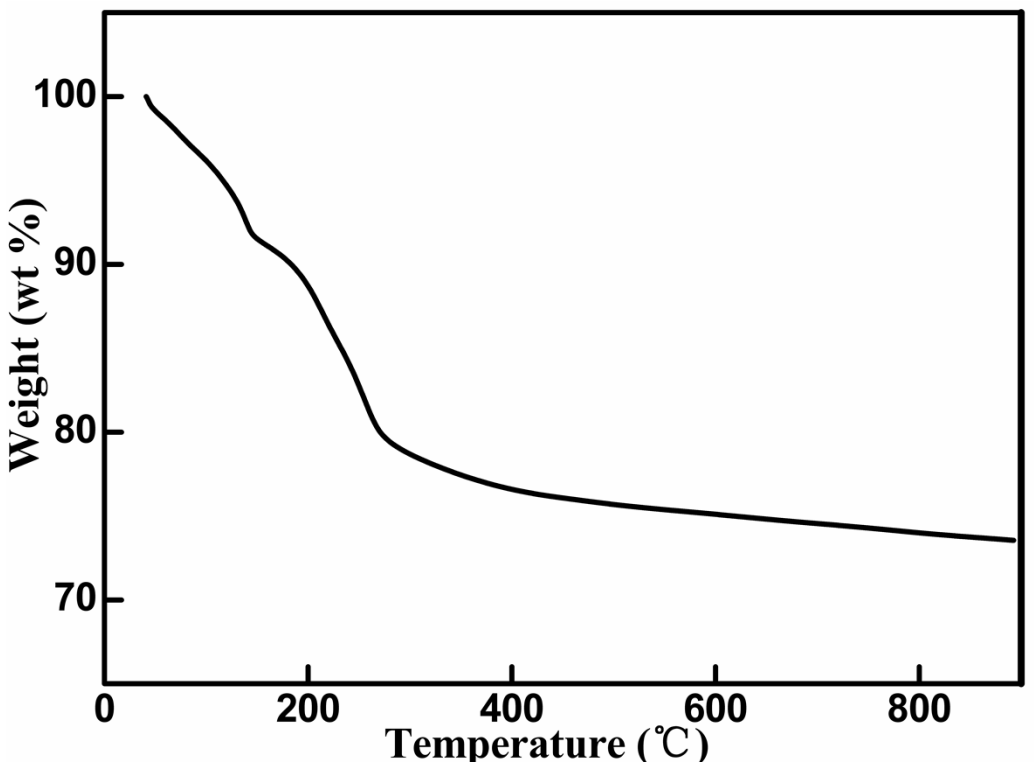

Fig. S2 Thermogravimetric analysis (TGA) of the as-prepared Ni-Co-Mn-based precursors.

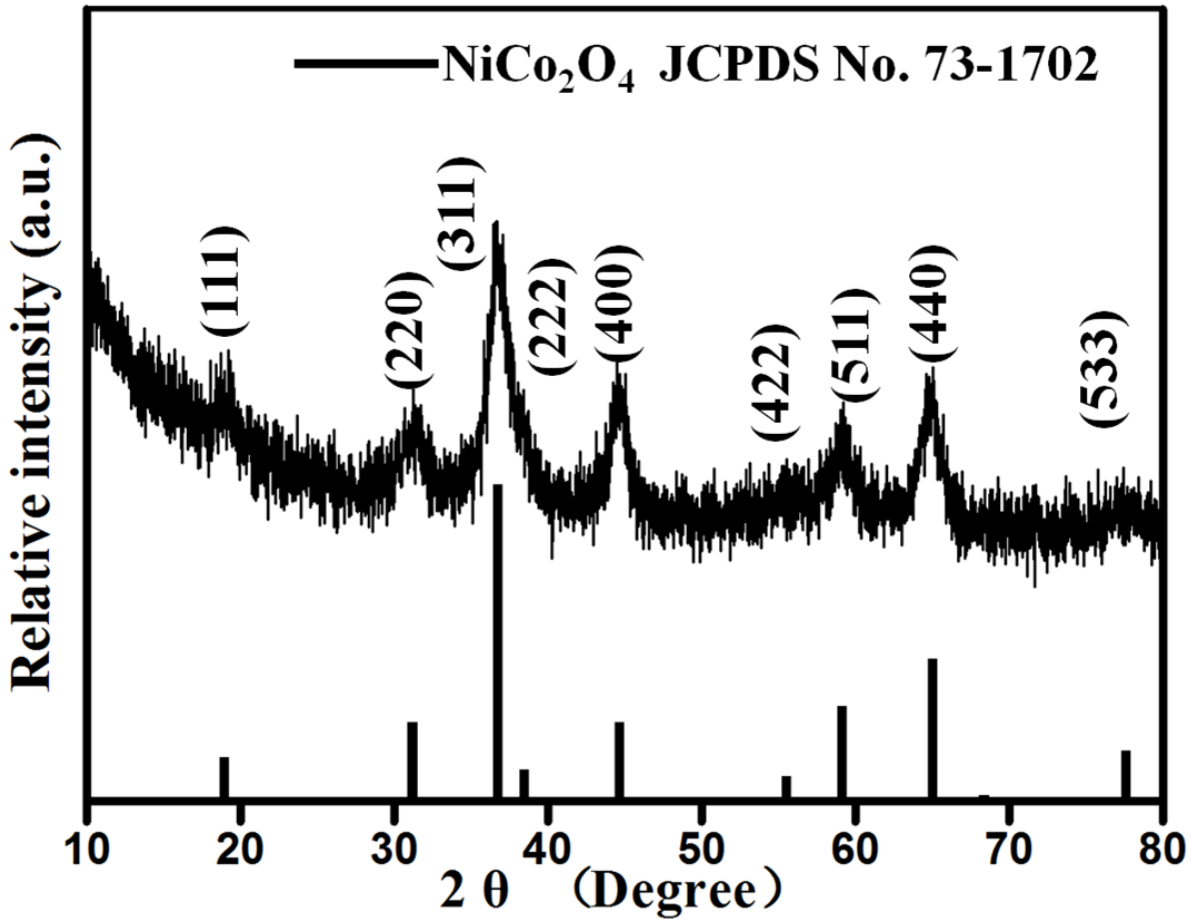

Fig. S3 XRD patterns of as-prepared pure $NiCo_2O_4$.

Tab. S1 Some diffraction peak positions of the prepared $NiCo_2O_4/MnCo_2O_4$, $NiCo_2O_4$, $NiCo_2O_4$ (JCPDS card no. 73−1702) and $MnCo_2O_4$ (JCPDS card no. 23−1237).

Samples	2θ (degree)						
	(111)	(220)	(311)	(400)	(422)	(511)	(440)
$NiCo_2O_4/MnCo_2O_4$	18.66	30.76	36.35	44.20	54.87	58.49	64.28
$NiCo_2O_4$	19.03	31.37	36.71	44.59	54.40	59.18	64.94
$NiCo_2O_4$ (JCPDS no. 73-1702)	18.928	31.152	36.705	44.635	55.431	59.115	64.963
$MnCo_2O_4$ (JCPDS no. 23-1237)	18.547	30.537	35.995	43.759	54.336	57.909	63.622

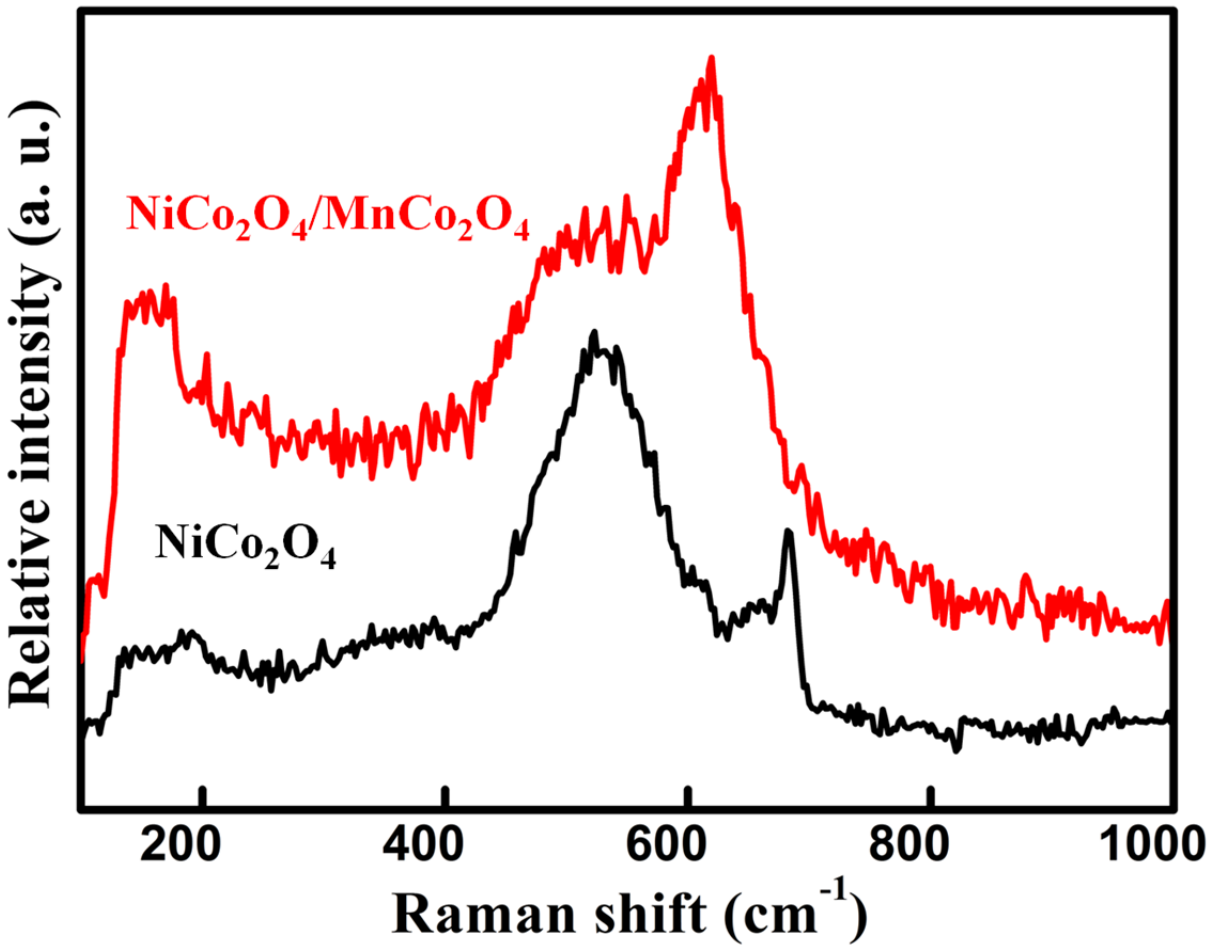

Fig. S4 Raman spectra of $NiCo_2O_4/MnCo_2O_4$ and $NiCo_2O_4$ excited with 473 nm laser.

Tab. S2 The Raman peak positions of the synthesized products and previously reported $NiCo_2O_4$, $MnCo_2O_4$ and manganese-based oxides.

Sample	Raman shift (cm^{-1})									Ref.
$NiCo_2O_4$/ $MnCo_2O_4$	184 202	-	-	481	516 532	549	622	-	-	This work
$NiCo_2O_4$	195	-	-	458	523	543	-	683	-	This work
$NiCo_2O_4$	219	-	-	473	-	552	-	676	-	17
$NiCo_2O_4$	186	-	-	456	504	-	648	-	-	18
$MnCo_2O_4$	200	-	-	480	520		667	680	-	19
$MnCo_2O_4$	188	-	-	492	-	567	668	-	-	20
α-Mn_2O_3	-	-	396	-	-	-	-	690	-	
Mn_3O_4	-	291	375	480	-	-	-	657	-	21
β-MnO_2	162	-	-	-	-	538	-	667	750	

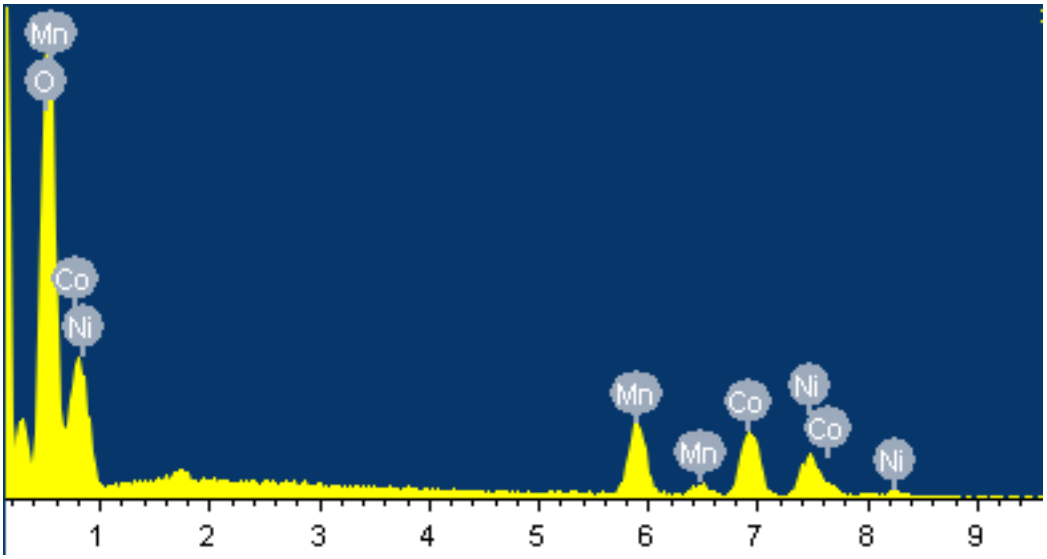

Fig. S5 EDS spectrum of $NiCo_2O_4/MnCo_2O_4$.

Tab. S3 the interplanar spacing **of** the prepared $NiCo_2O_4/MnCo_2O_4$, $NiCo_2O_4$ (JCPDS card no. 73-1702) and $MnCo_2O_4$ (JCPDS card no. 23−1237).

Samples	D (Å)				
	(440)	(511)	(400)	(311)	(220)
$NiCo_2O_4/MnCo_2O_4$	1.47	1.61	2.08	2.51	2.94
$NiCo_2O_4$ (JCPDS no. 73-1702)	1.43	1.56	2.03	2.45	2.87
$MnCo_2O_4$ (JCPDS no. 23-1237)	1.46	1.59	2.07	2.49	2.92

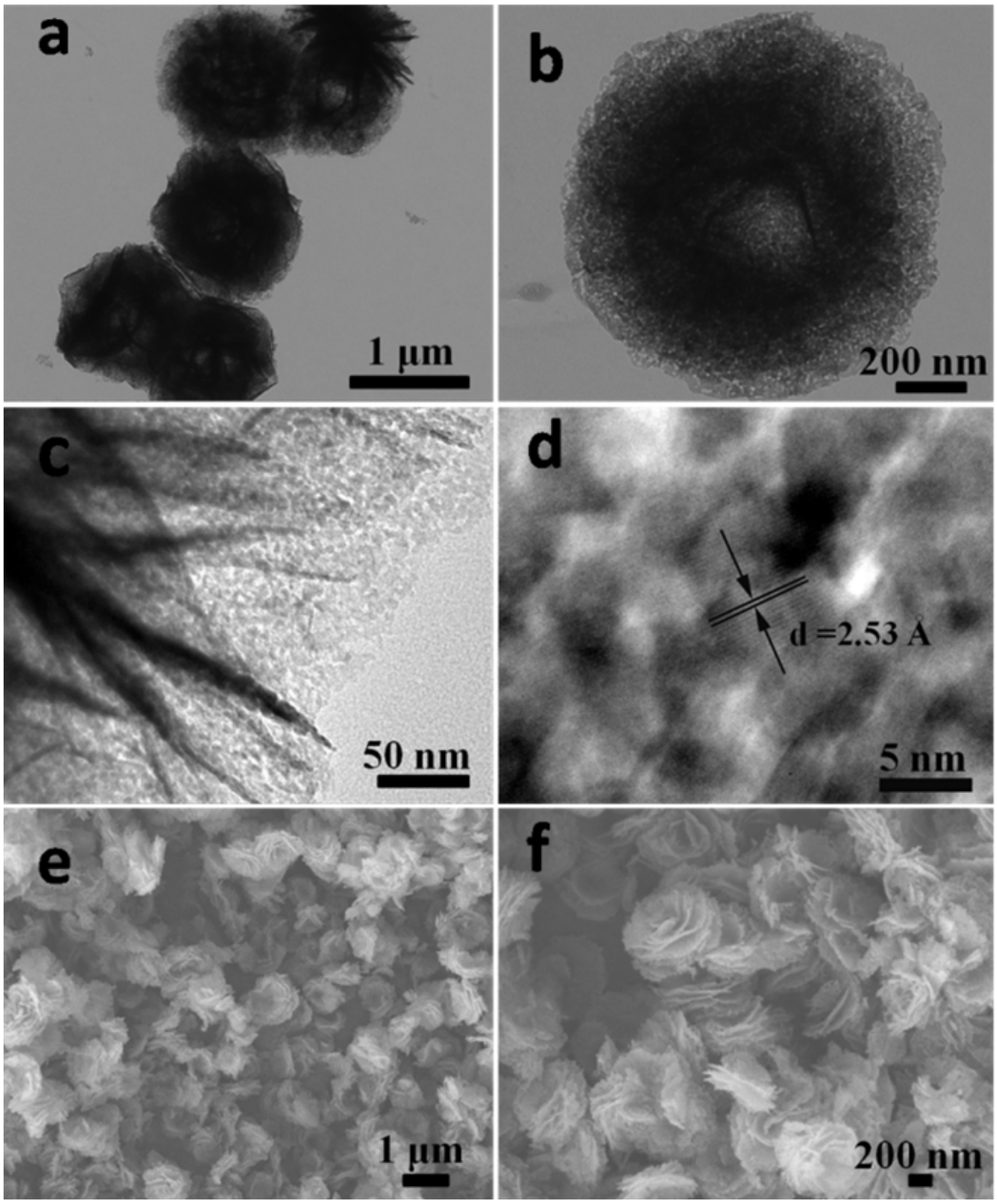

Fig. S6 (a, b, c) TEM images, (d) HRTEM image and (e, f) SEM images of the as-prepared mesoporous $NiCo_2O_4$ hierarchical architectures.

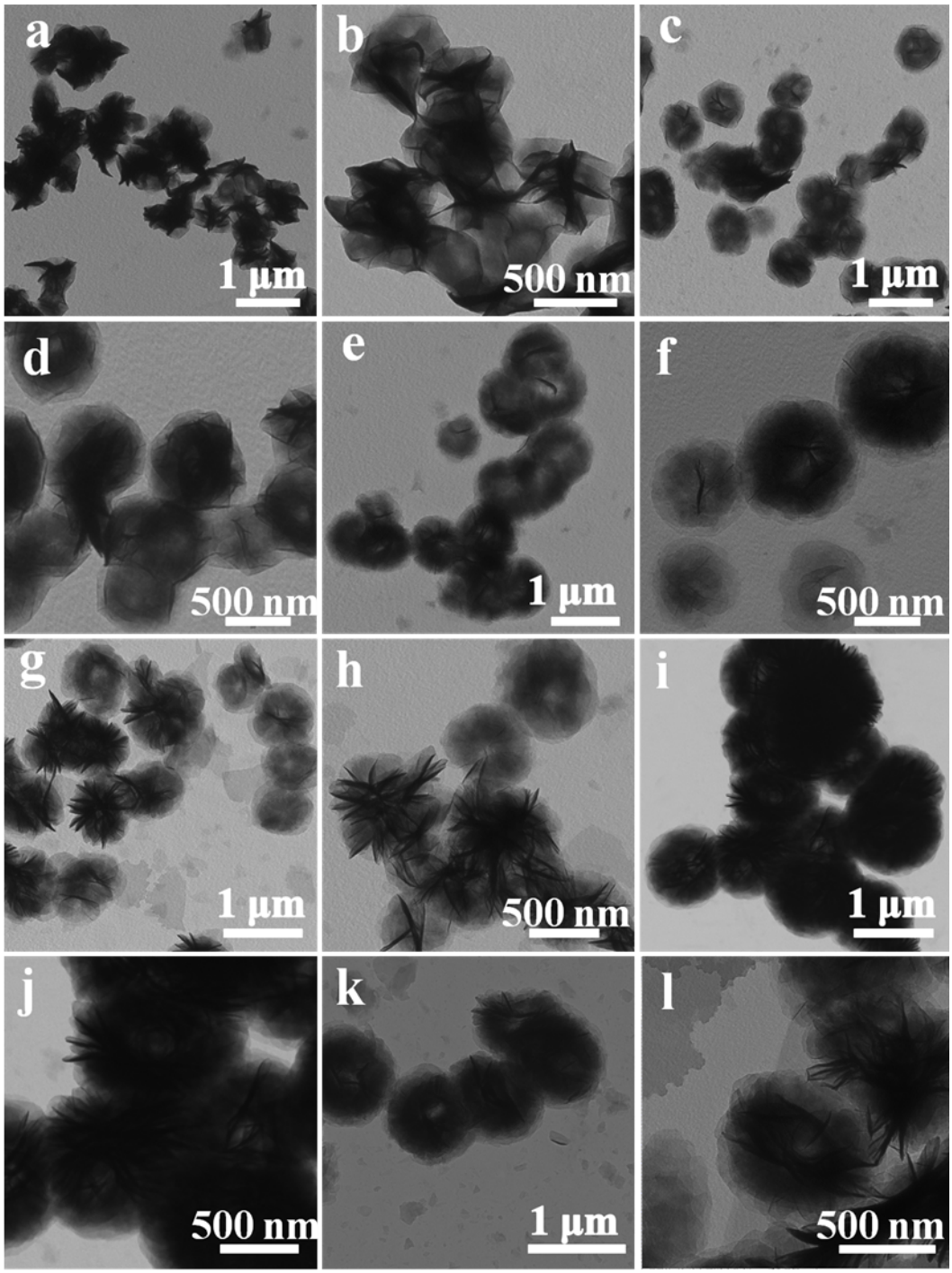

Fig. S7 TEM images of the Ni-Co-based precursors synthesized at 180 ºC for (a, b) 40 min (c, d) 50 min, (e, f) 2.0 h, (g, h) 5.0 h, (i, j) 12.0 h and (k, l)15.0 h.

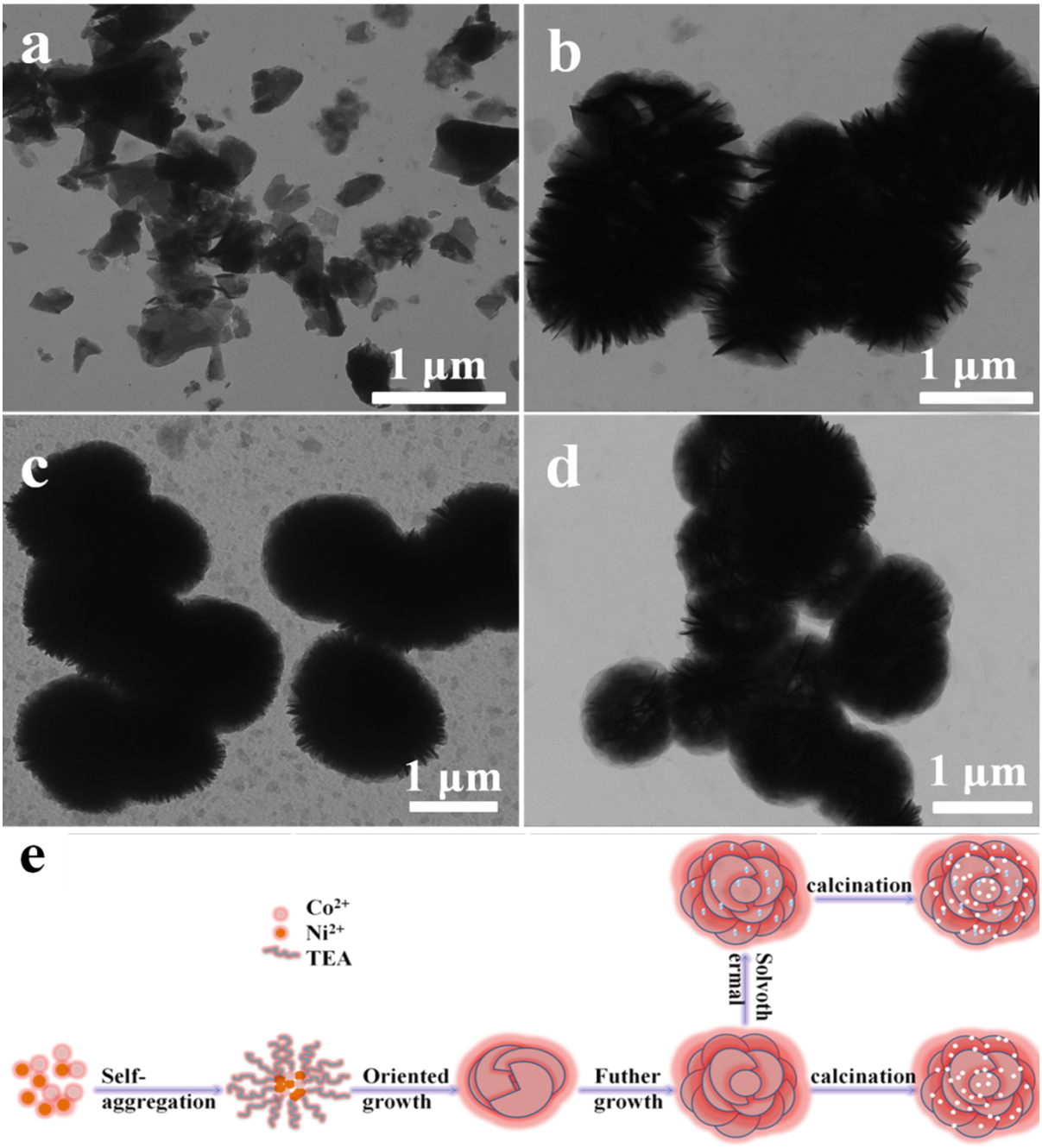

Fig. S8 TEM images of the Ni-Co-based precursors synthesized with different amounts of TEA: (a) 0 ml, (b) 3 ml, (c) 6 ml, (d) 10 ml at 180 ºC while keeping other experimental parameters unchanged; (e) the possible formation mechanism of the 3D hierarchical porous rose-like architectures.

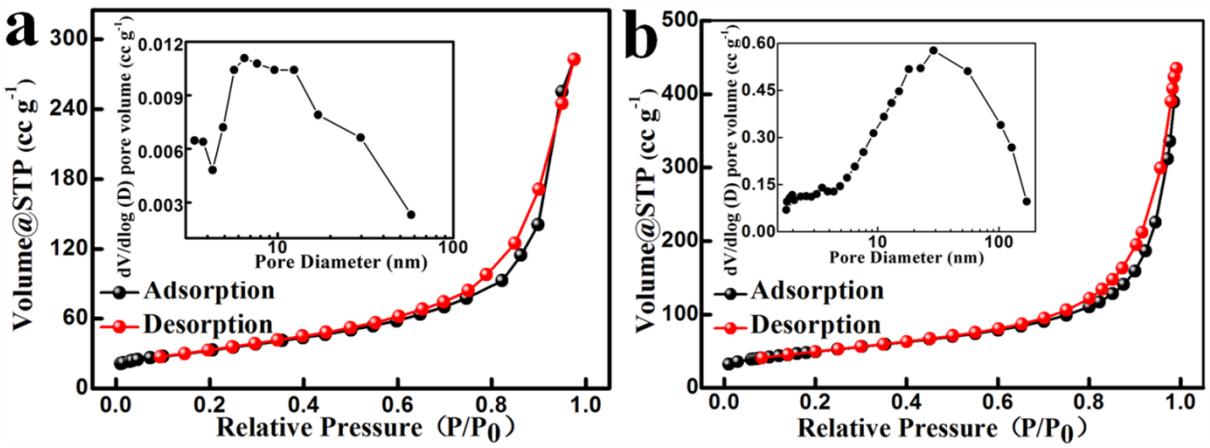

Fig. S9 Nitrogen adsorption-desorption isotherm and the corresponding pore size distribution (inset) of (a) hierarchical porous rose-like $NiCo_2O_4$ and (b) hierarchical porous rose-like $NiCo_2O_4/MnCo_2O_4$.

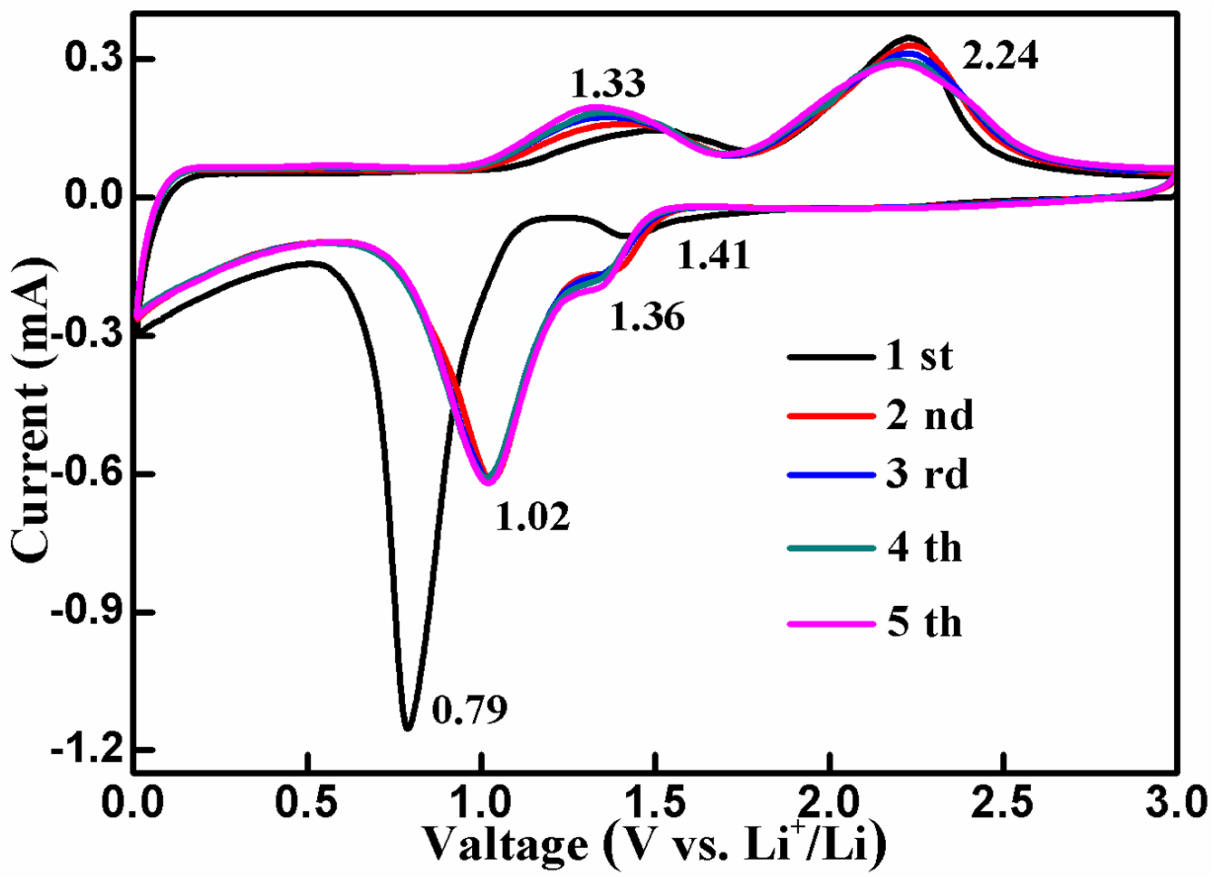

Fig. S10 The first five cyclic voltammogram curves of the 3D hierarchical porous rose-like $NiCo_2O_4$.

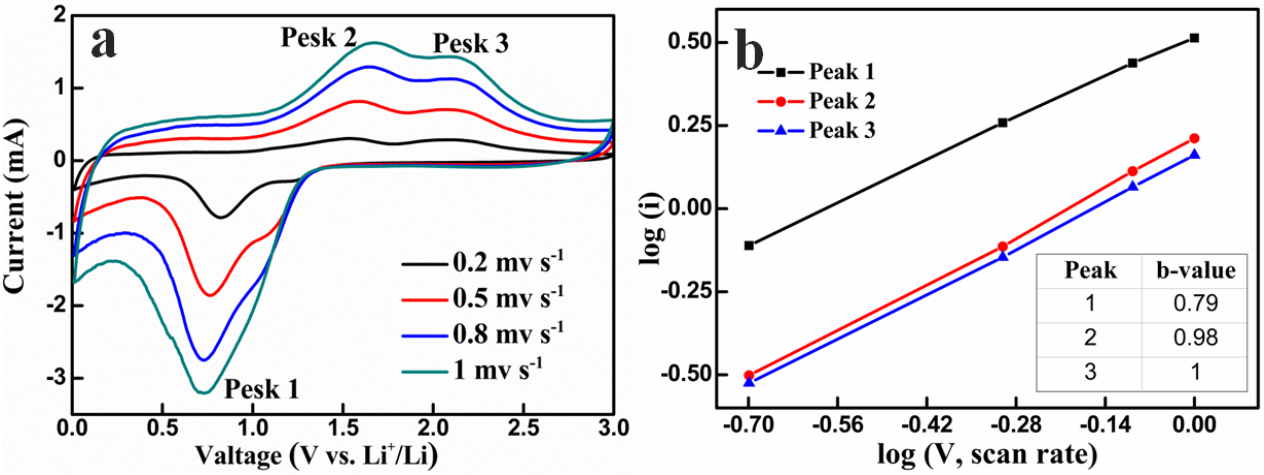

Fig. S11 (a) CV curves of $NiCo_2O_4/MnCo_2O_4$ at different scan rate after 350 cycles and (b) logi vs. logv plots at different peaks.

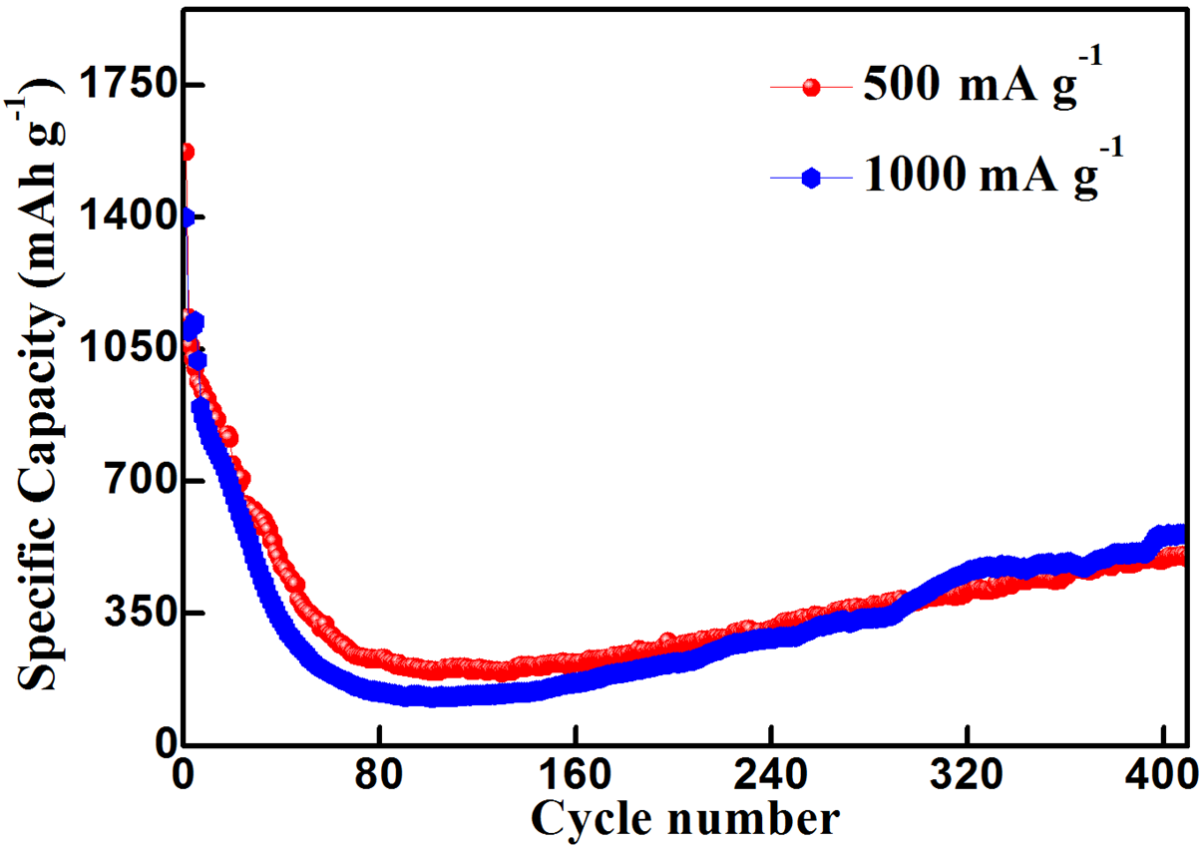

Fig. S12 Cycling performance of $NiCo_2O_4/MnCo_2O_4$ with active materials of 70 % at 500 and 1000 mA g^{-1}.

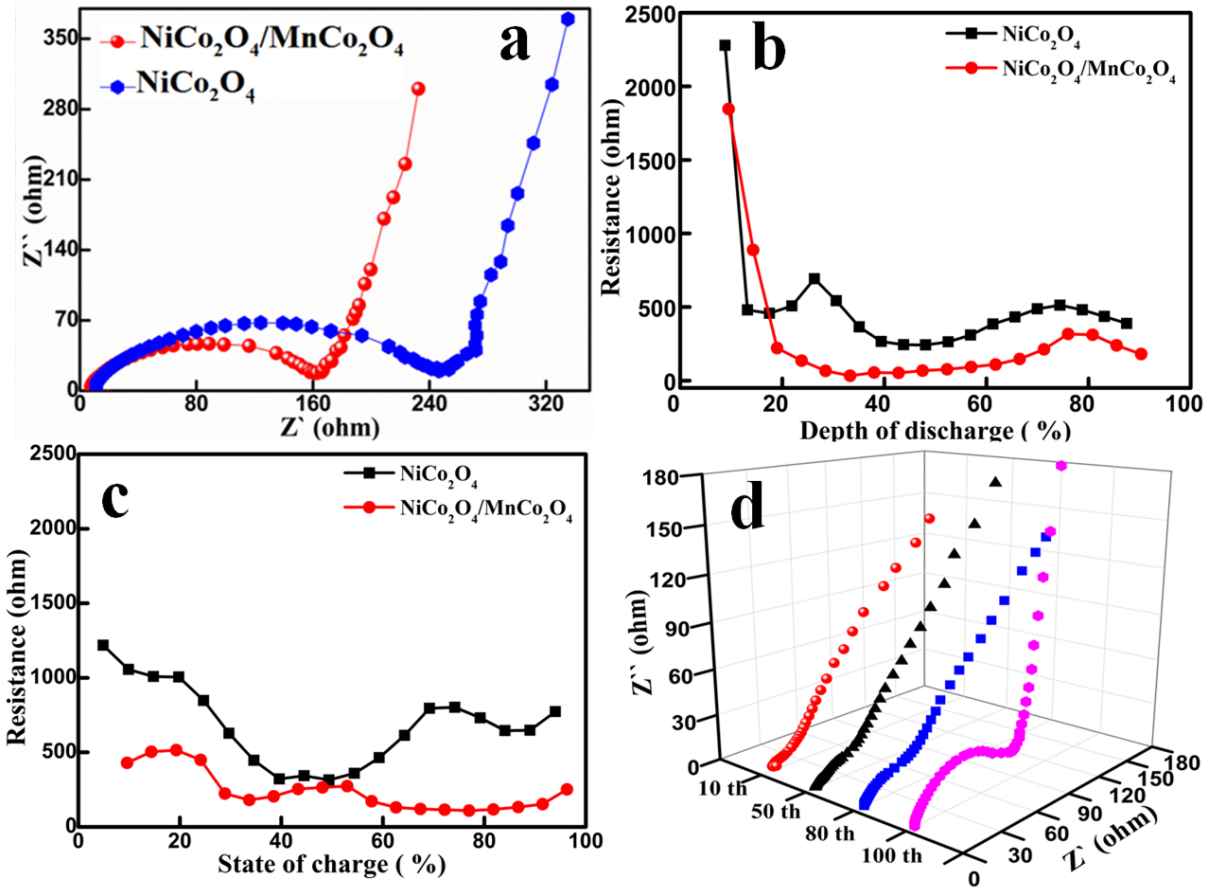

Fig. S13 (a) Nyquist plots of the AC impedance spectra measured over the frequency ranging from 100 kHz to 0.01 Hz and (b, c) the direct current resistance (R_{dc}) for the $NiCo_2O_4/MnCo_2O_4$ and $NiCo_2O_4$ electrodes. (d) The AC impedance spectra of the $NiCo_2O_4/MnCo_2O_4$ after certain cycles at 1000 mA g^{-1} in the frequency ranging from 100 kHz to 0.01 Hz.

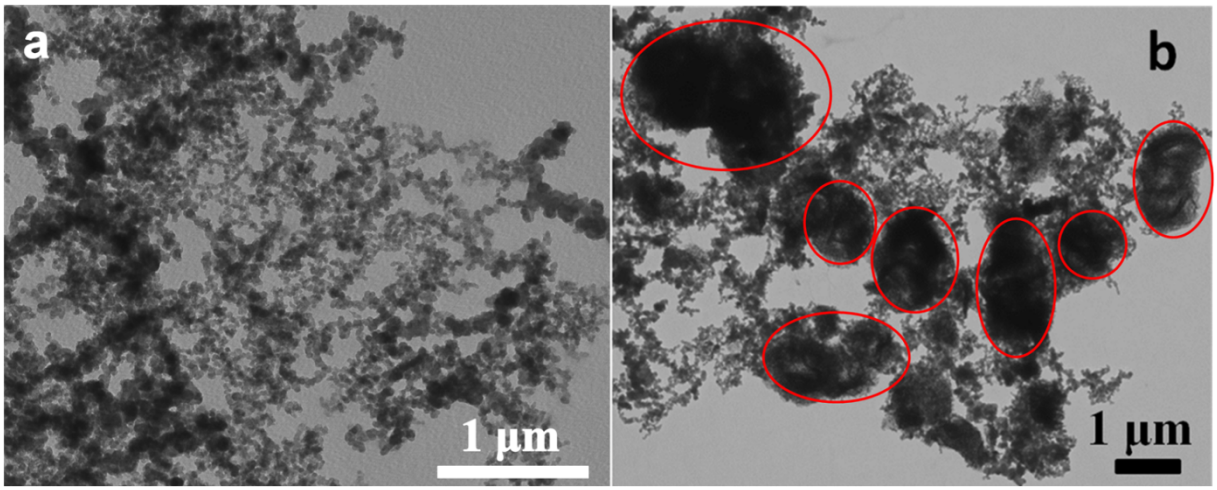

Fig. S14 (a) TEM image of the acetylene-black used as active material and (b) TEM image of $NiCo_2O_4/MnCo_2O_4$ composite used as active material (marked by the red frame) and acetylene-black acted as conductive agent after ten cycles at a current density of 1000 mA g^{-1}.